# Resilience-oriented decision making on the pre-shock intervention to road networks

Siyao Yang[1,7], Li Sun[3,7*], Gang Li[1,2*], John Shawe-Taylor[4,5], Haijiang Li[3], and Božidar Stojadinović[6]

[1]State Key Laboratory of Structural Analysis Optimization and CAE Software for Industrial Equipment, Department of Engineering Mechanics, Dalian University of Technology, Dalian 116024, China;
[2]Ningbo Institute of Dalian University of Technology, No. 26, Yucai Road, Jiangbei District, Ningbo 315016, China;
[3]School of Engineering, Cardiff University, Cardiff, CF24 3AA, United Kingdom;
[4]Artificial Intelligence Centre, University College London, London, WC1E 6BT, United Kingdom;
[5]International Research Centre on Artificial Intelligence (IRCAI), Jožef Stefan Institute, 1000 Ljubljana, Slovenia;
[6]Department of Civil, Environmental and Geomatic Engineering, ETH Zürich, 8093, Zürich, Switzerland;
[7]These authors contributed equally: Siyao Yang, Li Sun;
*E-mail: sunl32@cardiff.ac.uk; ligang@dlut.edu.cn.

**Abstract**: Pre-shock intervention (PSI) has emerged as a proactive and promising approach to enhancing the resilience of critical infrastructure systems (CISs) against natural disasters. However, optimizing the decision-making on the PSI of real-world CISs is often challenging due to the inherent uncertainty of disaster events, as well as the fragility and recoverability of the physical systems. To address this challenge, this research introduces a search-based decision-making (**SBDM**) framework of selecting and scheduling PSI as a resilience amelioration tool of CISs, with a specific emphasis on road networks (RNs) subjected to damaging earthquakes. Accordingly, seismic performance enhancement of bridge structures has been adopted as a viable PSI approach, aiming to reduce their fragility while also facilitating the emergency restoration (ER) of RNs in the immediate aftermath of earthquakes. To quantify the impact of different selected and scheduled PSI lists on seismic resilience of RNs, an agent-based model (ABM) is developed to track the PSI-driven ERs and integrated into the **SBDM** framework. In this ABM, each recovery team involved in the ER campaign is modelled as an agent with behaviour determined by predefined attributes. Given a particular PSI list, the initial damage status of the RN under any given earthquake scenario is obtained, while the subsequent post-earthquake ER trajectory is also shaped by the ABM. Hence, the total loss of the whole RN is assessed. An optimal PSI list is thereafter identified by the **SBDM** framework as the one that best enhances seismic resilience of the RN. To examine its applicability, this **SBDM** framework is employed to guide the PSI of a real-world RN. Case study results demonstrate that the PSI list derived from the **SBDM** framework consistently outperform those derived from the intuition-driven, baseline strategies across diverse earthquake scenarios, underscoring its robustness.

**Keywords**: Resilience; Emergency restoration; Pre-shock intervention; Agent-based model; Decision-making; Road network

# 1. Introduction

Critical infrastructure systems (CISs), including transportation, energy, communication, and water systems, serve as the backbone of urban communities (Thacker et al. 2019). As these systems grow increasingly complex and interdependent (Helbing 2013), even localized damage of any single CIS can propagate and potentially trigger a cascading failure across the entire network (Buldyrev et al. 2010; Brummitt et al. 2012; Bashan et al. 2013; Zhao and Sun 2021). This inherent vulnerability of modern CISs is further exacerbated by the growing frequency and intensity of natural disasters, driven by climate change (Druckenmiller et al. 2024).

Among various natural disasters, earthquakes pose a particularly grave threat to CIS resilience due to their unpredictability and capacity for widespread disruption. For example, the 2023 Turkey-Syria earthquakes resulted in over 50,000 fatalities and caused approximately $84.1 billion in the economic losses in Turkey alone (Aktas et al. 2023). The observation on major earthquake disasters worldwide has highlighted that a critical barrier to seismic resilience lies in the inability of state-of-the-practice disaster management systems to deliver prompt and sound recovery in the immediate aftermath of earthquakes (IAoEs). To address this challenge, the post-shock emergency restoration (ER) that aims to minimize the functionality losses of CISs in the IAoEs and mitigating the exacerbation of earthquake-initiated damage, has been explored as a novel pathway towards future resilient CISs (Sun et al. 2021, Sun et al. 2022).

Nevertheless, it would be challenging for the ERs to be planned and executed across the interwoven CIS-urban community, in the wake of catastrophic earthquakes. In IAoEs, real-time data on earthquake-induced damage is often difficult to obtain, incomplete, or inaccurate (Noh et al. 2020, Luo and Paal 2021), leading to misguided ER efforts. Additionally, the mobilization of physical, human, and financial resources for ER operations is often constrained in such a period, particularly in the face of widespread destructions (Galasso and Opabola 2024, Mesta et al. 2025). Furthermore, while ER can mitigate socio-economic losses, it cannot reverse the irreversible loss of human lives resulting from structural collapses (Zhang et al. 2012, Arslanturkoglu and Stojadinovic 2022, Zhao et al. 2023, Mesta et al. 2025), including failures of buildings and critical CIS components such as bridges in road networks (RNs).

In this context, pre-shock intervention (PSI) has emerged as a proactive and cost-effective strategy to enhance the resilience and sustainability of CISs against natural disasters (Chang et al. 2012). Unlike post-shock ERs, PSIs enable the implementation of targeted mitigation measures prior to disaster events, thereby reducing structural vulnerabilities (Venkittaraman and Banerjee 2014) and lowering the risk of cascading, system-wide failures (Wu and Chen 2023). However, applying PSI to all components in a CIS would demand substantial resources and entail prohibitive costs. Moreover, since individual components contribute unequally

to the overall functionality and resilience of the system, a blanket PSI is neither practically feasible nor economically justifiable (Huang et al. 2014; Nicholson et al. 2024).

To address this challenge, a growing body of research has been undertaken to develop principled decision-makings that maximize the benefit of PSI of CISs subjected to natural disasters.

Dong et al. (2014) developed a decision-making framework to support the sustainability-oriented, pre-earthquake retrofit of RNs. In this framework, sustainability is quantified by the expected economic losses associated with potential seismic events, while the total cost of the retrofit denotes the economic investment required to improve seismic resilience of the network. These two objectives—minimizing seismic-induced economic losses and limiting retrofit expenditures—are characterized as conflicting criteria. To resolve this trade-off, a multi-objective optimization approach is employed to derive optimal strategies for sequencing and timing the system-level retrofit campaign across the RN.

Zhang and Wang (2016) introduced the weighted independent pathways (WIPW) as a novel performance metric of RNs, in the context of pre-shock bridge retrofit planning. This metric integrates multiple key attributes of the network, including its topological configuration, redundancy levels, traffic flow patterns, and the seismic fragility of individual bridges. Accordingly, a ranking mechanism is proposed in this study to identify the pre-shock retrofit scheme that is most effective to the risk mitigation of the RN subjected to damaging earthquakes.

Silva-Lopez et al. (2022) presented a neural network surrogate model that enables a rapid and accurate estimation of changes in traffic performance metrics of modern RNs due to the earthquake-initiated damage of bridge structures. In parallel, a modified version of the local interpretable model-agnostic explanation (LIME) is proposed as a retrofit strategy that minimizes the impact of seismic disasters on the RN. With the RN across San Francisco Bay Area as a testbed, the neural network is found to be able to accurately predict the system's performance with significantly reduced computation time, thereby enabling decision-makers to assess the impact of bridge retrofit within the network. Besides, based on the newly-proposed LIME-TI metric, those bridges whose retrofit can effectively enhance the robustness of the RN can be identified.

Most recently, Bhattacharjee and Baker (2023) introduced a global variance-based sensitivity analysis to support the prioritization of bridge retrofits within regional RNs exposed to uncertain seismic hazards. For each individual bridge, this method utilizes total-order sensitivity indices (Sobol' indices) to quantify the influence of its retrofit status on the variance in the expected disruption cost across the entire RN. In particular, this approach also accounts for the influence of the interaction between the retrofit status of different bridges. Following the case-study on a RN in San Francisco, which consists of a total of 71 highway bridges, the new method demonstrated its capacity to generate a retrofit prioritization strategy that incorporates the probabilistic nature of seismic events, the uniqueness of individual bridges, network effect, and the preferences of decision-makers**.**

It is noteworthy that, apart from vulnerability mitigation, PSIs could also enhance the recoverability of bridge structures (Luo et al. 2025), as another pillar of disaster resilience (Bruneau et al. 2003). However, this impact has not been explicitly integrated into the decision-making on the PSl, by the aforementioned research. To narrow this knowledge gap, some studies have been conducted to develop a decision-making framework on the resilience-oriented PSI of CISs, incorporating both vulnerability mitigation and recoverability enhancement. Notably, Jafari et al. (2024) proposed an optimization-based decision-making framework to guide resource allocation aimed at bolstering the seismic resilience of RNs subjected to mainshock–aftershock sequences. This framework considers both pre-shock retrofit and post-shock restoration of bridges, explicitly incorporating the accumulation of damage caused by aftershocks. A case study was conducted using a virtual RN composed of six bridges, exposed to a magnitude 7.5 mainshock followed by three aftershocks. The results produced an array of optimal solutions that features the trade-off between competing objectives, such as cost minimization and resilience maximization. This allows disaster managers to make informed decisions aligned with their resilience goals and budgetary constraints.

Notwithstanding the new insights generated from the state-of-the-art research, the looped and dynamic interdependence between diverse recovery activities—particularly in the IAoEs—remains underexplored in the context of PSI planning (Sun et al. 2021). To address this gap, this study introduces a search-based decision-making (**SBDM**) framework that aims to optimize the selecting and scheduling of PSIs, with a particular focus on RNs, which often constitute a lifeline for urban communities under natural disasters. The proposed framework adopts seismic performance enhancement of bridge structures as a viable and principal PSI approach. Such an approach aims not only to reduce bridge fragility but also to facilitate rapid repairs—an essential ER of RNs in IAoEs. The updated fragility model of bridge structures, where the PSI is implemented, is incorporated into the **SBDM** framework. In parallel, to enable a nuanced assessment of the impact of different PSI lists on seismic resilience of the RN, an agent-based model (ABM) is developed to simulate post-shock ERs (Costa et al. 2021, Sun et al. 2021, Sharif et al. 2023, Sun et al. 2025) and integrated into the **SBDM** framework. Given a particular PSI list, this framework can therefore examine its impact on both vulnerability and recoverability of the RN. Consequently, the optimal PSI list, out of the entire search space, is identified by this framework as the one that best enhances seismic resilience of the RN.

The remainder of the paper is organised as follows: Section 2 introduces the **SBDM** framework; Section 3 introduces a real-world RN as the test bed, where the framework is applied; Section 4 presents and discusses the outcome of the case-study; Finally, Section 5 draws the main conclusions.

## 2. The search-based decision-making framework

In this study, the PSI focuses upon the seismic performance enhancement of bridges, which—despite being one of the most crucial components of modern RNs—are often found to be vulnerable under damaging earthquakes (Mackie et al. 2010, Kilanitis and Sextos 2019). Accordingly, as a proactive strategy, the PSI would mitigate the earthquake-induced damage to bridges during the absorption phase (El-Hawat et al. 2022, Shen et al. 2024), while also facilitating the rapid and effective repair (Nie et al. 2025).

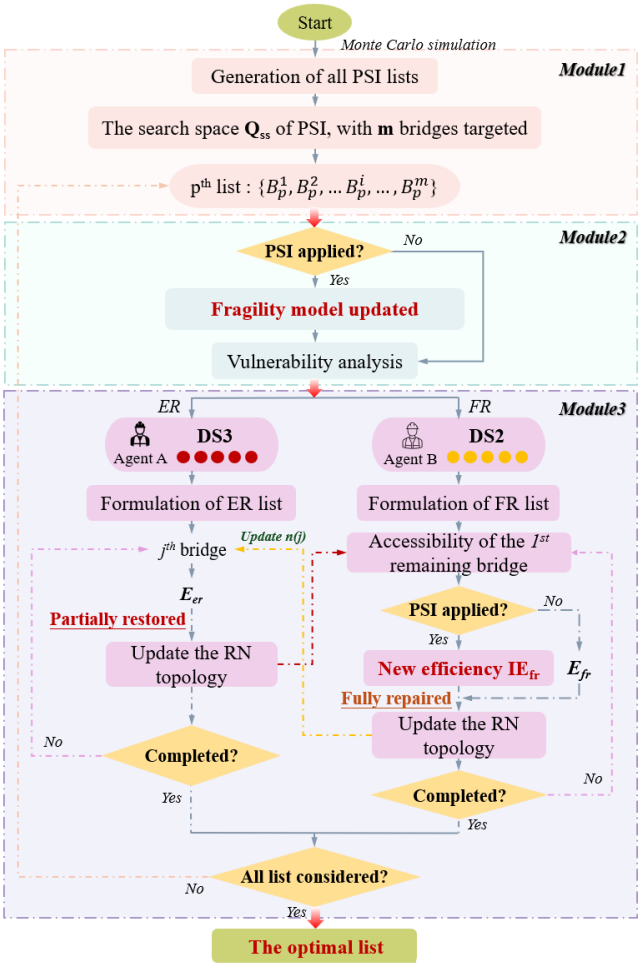


Figure 1. The **SBDM** framework on the PSI of RNs.

It is worth noting that, the key challenge facing PSI decision-making is how to balance the trade-off between the fragility and criticality of bridges of the RN under consideration. Regarding modern RNs, high-priority bridges are not only vital to the minimization of earthquake-initiated losses, but also the rapid functionality recovery thereafter. However, by and large, these bridges are often designed following state-of-the-art seismic codes, and ultimately, sufficiently robustness. Therefore, it might not be that cost-effective to invest PSI resources on them, notwithstanding their criticality (Carturan et al. 2013).

On the other hand, vulnerable bridges are often not playing a significant role regarding the connectivity of RNs, and thus not justifying PSI costs either, as their failure usually tends to have a marginal impact on the overall network functionality.

To navigate this complexity, this newly-developed **SBDM** framework loops the impact of PSI on both vulnerability and recoverability into the decision-making. To that end, the framework is structured into three modules: (1) generation of the search space of PSI, (2) PSI-driven seismic vulnerability analysis, and (3) PSI-driven functionality recovery in the IAoEs, as illustrated in Fig. 1.

Lastly, by backpropagating the total loss regarding each of the potential PSI list out of the whole search space, the optimal list, *i.e.*, the one associated with the minimum loss, will be identified by the framework.

## 2.1. Generation of the search space of PSI

To support the search-based decision-making, Module 1 is dedicated to constructing the complete search space, which comprises all potential PSI lists. This space is constructed through combinatorial enumeration, whereby each PSI list corresponds to a unique subset of bridges. Let $B = \{B_1, B_2, \dots, B_N\}$ denote the set of all the bridges in the RN under consideration, totalling $N$. In case of resource constraints, it is often assumed that only $m$ bridges ($m \leq N$) can be selected for the PSI. The search space is therefore defined by the combinatorial selection of $m$ bridges from the $N$ available ones in the RN. Mathematically, the quantity of the potential PSI lists included in this search space, denoted as $Q_{ss}$, can be obtained by Eq. (1):

$$Q_{ss} = \binom{N}{m} = \frac{N!}{m!(N-m)!} \tag{1}$$

As shown in Fig. 1, $B_p^i$ refers to the $i^{th}$ bridge ($i$ = 1, 2, …, $m$) incorporated into the $p^{th}$ list, among the total of $Q_{ss}$ generated combinations.

Despite the reduction from $N$ to $m$ bridges, the value of $Q_{ss}$ can still be substantial, especially for large-scale RNs, leading to prohibitive computational costs. To mitigate this computational burden while ensuring informed decision-making, this study introduces a Weighted Promise Index (WPI) as a pre-screening metric. The WPI quantifies the "promising" nature of each bridge with respect to its inclusion in the PSI, by integrating both its fragility and criticality. Bridges exhibiting both high fragility and criticality are considered more impactful for the PSI, as their performance enhancement is likely to significantly improve the system-level resilience. In this study, regarding each bridge $B_k$ ($k$ = 1, 2, …, $N$), its WPI, denoted as $WPI_k$, is computed following Eq. (2):

$$WPI_k = \alpha \times NBW_k + (1- \alpha) \times P_c(k) \tag{2}$$

Here, $NBW_k$ stands for the normalized betweenness centrality of $B_k$, serving as a measure on the criticality of this bridge to the overall connectivity of the RN. This metric is computed by first determining the original

betweenness centrality value, $BW_k$, and then applying min–max scaling to rescale $BW_k$ to the interval [0, 1]. Meanwhile, $P_c(k)$ denotes the collapse probability of bridge $B_k$, derived from its seismic fragility model. The coefficient $\alpha \in [0,1]$ is a weighting factor that determines the relative importance given to the betweenness versus collapse probability in the *WPI* quantification.

Based on the WPI associated with each of the bridge, a more targeted and computationally affordable pre-screening process can be implemented, thereby streamlining the selection of bridges for the PSI list.

## 2.2. PSI-driven seismic vulnerability analysis

Module 2 assesses the functionality degradation of the RN resulting from earthquake-induced physical damage. Notably, only the damage of bridge structures is considered in this study, with the connecting road segments assumed to remain functional (Kilanitis and Sextos 2019). The assessment begins with a seismic fragility analysis to determine the damage state (DSs) of each bridge, using the intensity measure (IM) derived from ground motion attenuation models at each bridge's geographic location (Mackie and Stojadinovic 2006).

A total of three DSs are considered, namely, no damage (DS1), moderate damage (DS2), and collapse (DS3). To reflect structural variability across the RN, bridge-specific fragility models are employed, highlighting the influence of structural typology on seismic performance.

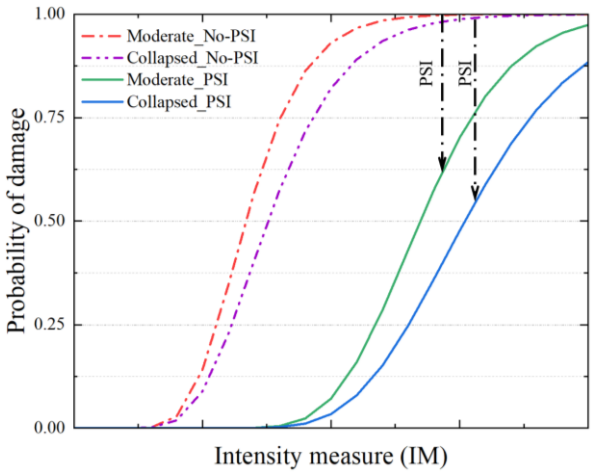


Figure 2. The impact of PSIs on the fragility behaviour of bridges.

In particular, to account for the impact of PSIs, the seismic fragility model of each relevant bridge is updated, as shown in Fig. 2. In this study, all fragility models are assumed to follow lognormal distributions (Karim and Yamazaki 2003). Accordingly, the two statistical parameters—mean and standard deviation—associated with DS2 and DS3 are adjusted following Eqs. (3-4), to underscore the enhanced seismic performance of the bridge (Lei et al. 2021, Martins and Silva 2021):

$$\mu_{updated} = \mu_{original} + \Delta\mu_{PSI} \tag{3}$$

In Eq. (3), $\mu_{original}$ and $\mu_{updated}$ denote the pre- and post-PSI mean values of the fragility function, respectively. The term $\Delta\mu_{PSI} \in [0,1]$ quantifies the enhancement in seismic performance due to the PSI, indicating a shift toward higher intensity levels required to induce the damage.

Likewise, the standard deviation is updated to capture reduced uncertainty in structural response following PSI implementation, as shown in Eq. (4):

$$\sigma_{updated} = \sigma_{original} \times \eta_{PSI} \tag{4}$$

Here, $\eta_{PSI} \in [0,1]$ serves as a reduction coefficient, indicating the extent to which variability in structural performance is reduced after the PSI. A lower $\eta_{PSI}$ suggests greater confidence in the improved seismic behaviour.

Based on the DS of a bridge under seismic hazards, its remaining functionality can be assessed. The functionality loss metrics developed by Gehl and D'Ayala (2018) is adopted in this study. Accordingly, it is assumed that bridges in DS3 are inaccessible to any vehicular traffic, while those ones in DS2 are passable but with reduced travel speeds, set at the 25% of their pre-shock level.

## 2.3. PSI-driven functionality recovery in the IAoEs

### 2.3.1. Agent-based model on the RN recovery

Module 3 addresses the post-earthquake recovery of the RN in the IAoE, shaped by two concurrent campaigns: ER and Full Repair (FR). As previously defined, the ER campaign aims at the rapid restoration of collapsed bridges, sometimes only to a minimally functional level (Sun et al. 2021), whereas the FR campaign focuses solely on restoring moderately damaged bridges to their original pre-shock capacity.

Notably, these two campaigns are interdependent, under real-world earthquake hazards. The efficiency of the ER squad may be compromised if it must traverse bridges still awaiting the FR, while the FR squad itself is delayed by the inaccessibility due to collapsed bridges—issues that only ER squad is equipped to resolve (Sun et al. 2021).

To account for this dynamic and cyclical interdependence, an agent-based model (ABM) is developed and integrated into the **SBDM** framework (Magoua et al. 2023). Within this ABM, the ER squad is designated as Agent A, responsible for the rapid restoration of collapsed bridge, while the FR squad is modelled as Agent B, tasked with repairing moderately damaged bridges. The behaviour of both agents in the IAoE is governed by pre-defined attributes (Sun 2017). Regarding Agent A, two key attributes—$E_{er}$ and $V_{er}$—denote its expected restoration efficiency and travel velocity, respectively. Similarly, the behaviour of Agent B is shaped by the two corresponding attributes, denoted as $E_{fr}$ and $V_{fr}$, respectively.

Once the collapsed and moderately damaged bridges have been identified following an earthquake, the ER and FR campaigns are initiated by Agents A and B, respectively. In the wake of real-world earthquake

disasters, the restoration time of each bridge is influenced by multiple interrelated factors—including the severity of the earthquake-induced damage, the accessibility, the structural characteristic, as well as the skilfulness and resourcefulness of the recovery squad. To systematically incorporate the effects of these variables within the **SBDM** framework, the time required to complete the ER of the $j^{th}$ collapsed bridge ($j$ = 1, 2, …, $N_c$, where $N_c$ stands for the total number of collapsed bridges), denoted as $RT_j$, is determined following Eqs. (5-6):

$$RT_j = TT_j + \frac{F_j}{E_{er} \cdot \omega^{n(j)}}, \quad if\ Span\ (j)\ \leq\ 50m\ or$$
$$RT_j = TT_j + \frac{F_j}{E_{er} \cdot \omega^{n(j)}} \cdot \left(\frac{Span(j)}{50}\right)^2, \quad if\ Span\ (j)\ >\ 50m, \tag{5}$$

with $j$ = 1:$N_c$, and

$$TT_j = \frac{SD_j}{V_{er}},\ for\ j = 1{:}\,N_c \tag{6}$$

Here, $TT_j$ refers to the time point at which Agent A reaches the $j^{th}$ collapsed bridge along its path. This is determined by $V_{er}$ and the shortest distance between the $(j-1)^{th}$ (the ER centre, when $j$ = 1) and $j^{th}$ bridges, denoted as $SD_j$. Consequently, the total restoration time of this bridge is the sum of $TT_1$ and the time required for the on-site restoration, as shown in Eq. (5).

In this **SBDM** framework, $F_j$ stands for the targeted functionality level of the $j^{th}$ collapsed bridge, characterized as the restored accessibility with an allowable travel speed reduced to 50% of its pre-shock level. Additionally, a discount factor $\omega^{n(j)}$, where $\omega$<1, is introduced to adjust $E_{er}$, based on the overall damage status of the RN. Mathematically, $n(j)$ denotes the total number of damaged bridges—in both DS2 and DS3—along the shortest path between the $(j-1)^{th}$ and $j^{th}$ bridges, *i.e.*, the last bridge restored by and the next bridge Agent A is heading to, respectively. Moreover, for bridges with spans exceeding 50 meters, the time required for the on-site restoration increases quadratically, to account for the rising engineering complexity (Yeh et al. 2015). Agent A proceeds iteratively, following Eqs. (5-6), until all collapsed bridges are restored.

In parallel, the FR campaign is executed by Agent B in a similar manner, based on its attributes $V_{fr}$ and $E_{fr}$. However, as noted earlier, the FR may be impeded by impassable routes resulting from collapsed bridges. In such cases, Agent B defers the campaign until Agent A restores the affected pathways, re-enabling the accessibility.

Lastly, in this paper, both Agents A and B follow a betweenness-based strategy, which always prioritizes bridges with the highest betweenness values, at each decision-moment, throughout the ER and FR campaign, respectively (Sun et al. 2025).

### 2.3.2. Impact of PSIs on the RN recovery

In addition to mitigating fragility, the PSI also enhances the recoverability of bridge structures following seismic events. To account for this impact, an improved efficiency parameter—denoted as $IE_{fr}$—is assigned to Agent B, when executing the FR of moderately damaged bridges that have undergone the PSI, as illustrated in Fig. 1.

By contrast, in the case of collapsed bridges, ER remains the primary intervention strategy in the IAoE, often involving the construction of temporary ramps or spans to restore the basic-level accessibility (Sun et al. 2021), as mentioned in Section 2.3.1. Accordingly, and consistent with Eq. (5), the time to complete the ER of a collapsed bridge is computed assuming an unchanged restoration efficiency $E_{er}$, irrespective of the PSI.

Nevertheless, it is vital to stress that, while PSI does not directly reduce ER times, the overall acceleration of the FR campaign—enabled by the prioritized selection of PSI-enhanced bridges—would have a knock-on effect on the ER. Ultimately, PSI contributes to the seismic resilience of the RN by fostering a synergistic recovery dynamic and promoting cohesive, time-effective endeavours across interdependent restoration pathways.

## 2.4. The resilience metric

In this study, the weighted connectivity loss (WCL) is included as the seismic resilience metric of RNs (Sun et al. 2022). Mathematically, given the selection of the $p^{th}$ PSI list in the entire search space ($p$ = 1, 2, …, $Q_{ss}$), the WCL of the RN under a given earthquake scenario, denoted as *WCL(p)*, is computed following Eq. (7):

$$WCL(p) = \sum_{t=0}^{T_c} \sum_{k=1}^{N} BW_k \times RS_{k,t}(p) \tag{7}$$

where $T_c$ refers to the time point at which both ER and FR campaigns are fully completed. Within this framework, *WCL* is quantified using a discrete-time approach, with a time step of 0.25 day. Meanwhile, $BW_k$ is obtained following the Eq. (8), in this **SBDM** framework:

$$BW_k = \frac{\sum_{s \neq k \neq t} \sigma_{st}(k)}{\sigma_{tot}} \tag{8}$$

Here, $\sigma_{tot}$ refers to the total number of shortest paths between all node pairs in the RN, while $\sigma_{st}(k)$ assumes a value of 1, if the shortest path between the nodes *s* and *t* traverses $B_k$, and 0 otherwise (Brandes 2001). The recovery state of $B_k$ at time point *t*, denoted as $RS_{k,t}(p)$, assumes the value of 0, 0.5, 2 and 4, which correspond respectively to: full recovery (or intactness), partial recovery (*i.e.*, the completion of ER, regarding collapsed bridges), moderate damage and collapse.

## 2.5. Scenario-based decision-making on the selection of PSI list

In light of the inherent unpredictability regarding both location and magnitude of future earthquake disasters, a scenario-based approach is adopted in this framework to support the decision-making. Specifically, each of

the PSI list drawn from the search space defined in Section 2.1 is examined under a comprehensive and diverse set of representative earthquake scenarios.

To further account for uncertainty in bridge structural fragility and recoverability, as well as the variation in the behaviour of the agents, a total of $N_{mc}$ Monte Carlo (MC) simulations are run, under each earthquake scenario. Ultimately, the optimal PSI list that is the one that minimizes the sum of the expected (*i.e.*, the mean of) WCL aggregated across all the scenarios, and denoted as $OPL_{expected}$, can be identified by Eq. (9):

$$OPL_{expected} = \underset{p \in Q_{ss}}{argmin} \sum_{q=1}^{N_{es}} EWCL_q(p) \tag{9}$$

$$EWCL_q(p) = \frac{1}{N_{mc}} \sum_{r=1}^{N_{mc}} WCL_q^r(p) \tag{10}$$

Here, $EWCL_q(p)$ denotes the expected WCL, conditioned upon the $q^{th}$ earthquake scenario ($q$ = 1, 2, …, $N_{es}$, where $N_{es}$ refers to the total number of earthquake scenarios incorporated) and the $p^{th}$ PSI list ($p$ = 1, 2, …, $Q_{ss}$). Meanwhile, as shown in Eq. (10), regarding the $q^{th}$ earthquake scenario, $WCL_q^r(p)$ stands for the WCL associated with the $r^{th}$ MC realization, among the $N_{mc}$ ones. Accordingly, $EWCL_q(p)$ can be obtained as the mean value of $WCL_q^r(p)$ ($r$ = 1, 2, …, $N_{mc}$).

To enhance the robustness of decision-making under extreme conditions, the **SBDM** framework also considers an alternative optimal PSI list, denoted as $OPL_{extreme}$. This list minimizes the aggregate 95$^{th}$ percentile of WCL, denoted as XWCL, across all earthquake scenarios, as shown in Eq. (11):

$$OPL_{extreme} = \underset{p \in Q_{ss}}{argmin} \sum_{q=1}^{N_{es}} XWCL_q(p) \tag{11}$$

$$XWCL_q(p) = WCL_q^{95}(p) \tag{12}$$

In this context, $XWCL_q(p)$ denotes the 95$^{th}$ percentile of WCL under the $q^{th}$ earthquake scenario and the $p^{th}$ PSI list, as defined in Eq. (12).

# 3. Case study

## 3.1. Configuration of the testbed RN

To validate its applicability, the **SBDM** framework outlined in Section 2 has been employed to support the decision-making on the PSI of a real-world RN in France, as the testbed. As depicted in Fig. 3, this hierarchical RN encompasses a route nationale (N125), multiple routes départementales, and local rural roads. In total, the RN consists of 118 bridges that connect 53 municipalities, including small villages and towns (Sun et al. 2022).

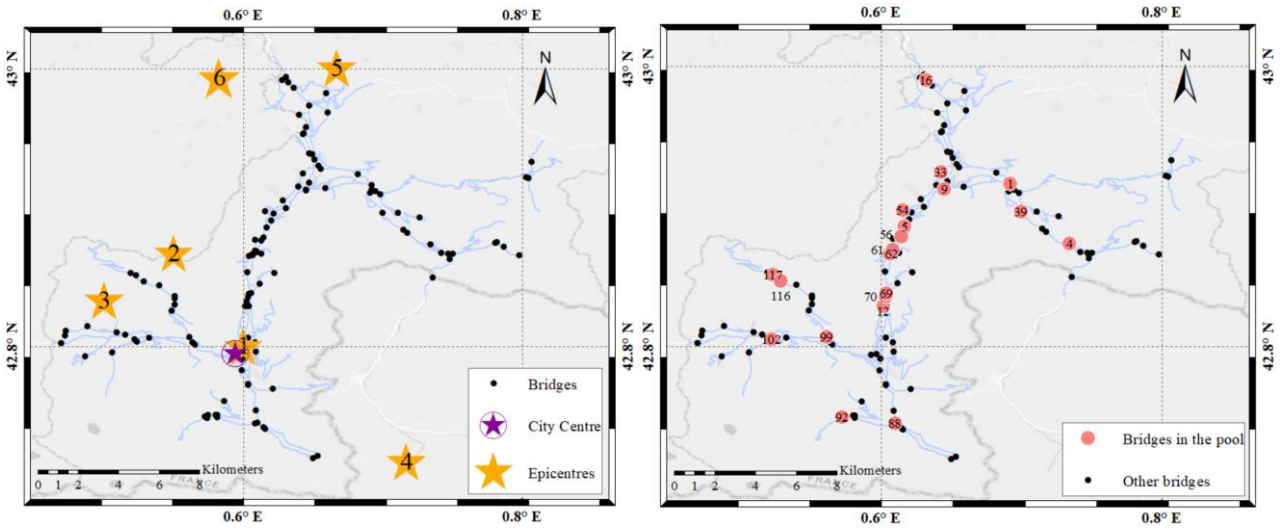


(a) The topology (b) The candidate pool

Figure 3. The testbed RN.

## 3.2. Search space of PSI lists

In this case-study, PSIs are assumed to be implemented with respect to 5 bridges within this RN, *i.e.*, $N = 118$, while $m = 5$, in Eq. (1).

Notably, to examine the effectiveness of the **SBDM** framework, two "greedy" decision-making strategies, which are fragility- and criticality-driven, respectively, are incorporated into this study, as the baseline. Following these two strategies, among all the 118 bridges in the entire RN, the 5 bridges with the highest collapse probabilities and the 5 with the highest betweenness centrality values are respectively selected for PSI.

Regarding the **SBDM** framework developed in this study, a preliminary selection process is conducted to identify a candidate set of 20 bridges for the potential PSI, to reduce the computational cost. Initially, the 10 bridges recommended by the two "greedy" strategies are all included into this set.

The remaining 10 are chosen from the other 108 bridges based on their WPIs, as defined in Section 2.1. In this case-study, $\alpha$ is set to 0.5 to ensure a balanced weighting between the fragility- and criticality-driven strategies, as shown in Eq. (2). Specifically, 6 bridges—comprising the three with the highest and the three with the lowest WPI values—are included to capture both ends of the spectrum of promise.

To further challenge the robustness of the **SBDM** framework, an additional 4 bridges are randomly selected from the remaining 102 bridges, enhancing the diversity of the candidate set, as illustrated in Fig. 3(b).

From a combinatorial perspective, this candidate pool of 20 bridges yields a total of 15,504 possible PSI lists, all of which are incorporated into the decision-making.

## 3.3. Scenario-based decision-making

To balance the trade-off between the comprehensiveness of the earthquake scenarios and computational tractability, three earthquake scenarios—corresponding to Epicentres Nos. 3, 4, and 5—are incorporated into the **SBDM** framework (*i.e.*, $N_{es}$ =3, in Eq. (9)), as illustrated in Fig. 3(a). In parallel, the remaining three epicentres (Nos. 1, 2, and 6) are designated as a test set to examine the performance of the optimal PSI list derived from the proposed **SBDM** framework. As detailed in Fig. 3, all six epicentres are selected based on the recorded historic seismic activity across the region, thereby ensuring the fidelity of the scenarios included.

Given their proximity to the central area of the RN, scenarios involving Epicentres Nos. 1 and 2 are anticipated to cause substantial damage. By contrast, the damage induced under earthquakes with Epicentre No. 6 is anticipated to be the least, among all the six ones, in light of its remoteness. Earthquakes originating from Epicentres Nos. 3, 4, and 5 are not projected to lead to widespread damage across the entire RN, but are expected to result in localized damage in the southwestern, southeastern, and northern areas, respectively, leading to a balanced decision-making.

In this case-study, regarding each scenario, a total of 200 MC simulations are run, following Eqs. (10) and (12), *i.e.*, $N_{mc}$ = 200. Given a particular PSI list, each MC realization starts with the generation of the initial damage scenario of the RN, via fragility analysis on all the bridges. To that end, as the IM on the ground motion at the geographic site of every individual bridge, the Peak Ground Acceleration (PGA) is computed following the attenuation model associated with a rock site, proposed by Campbell and Bozorgnia (2008). In accordance with the regional seismic source constraints and the validity range of the adopted attenuation model (up to $M_w$ = 7.5), the maximum seismic magnitude considered in this case study is set to 7.0 (Woessner et al. 2013).

In this case-study, the seismic fragility model proposed by Shinozuka et al. (2003) is applied to beam bridges, while the model developed by Zampieri (2014) is employed to examine the seismic behaviour of arch bridges. Meanwhile, as shown in Eqs. (3-4), to incorporate the influence of PSI on seismic fragility of bridge structures, the parameters of $\Delta\mu_{PSI}$ and $\eta_{PSI}$ are set to 0.7 and 0.75, respectively, regarding all the bridges, where PSI is implemented.

Table 1. Behavioural attributes of the agents.

| Agent | Attribute | Lower | Upper | Distribution | Average restoration time |
|---|---|---|---|---|---|
| *A* | $V_{er}$ (km/h) | 15 | 20 | Uniform | |
| | $E_{er}$ (%) | 50 | 100 | Uniform | 1.5days |
| *B* | $V_{fr}$ (km/h) | 5 | 10 | Uniform | |
| | $E_{fr}$ (%) | 5 | 10 | Uniform | 15 days |
| | $IE_{fr}$ (%) | 66.67 | 200 | Uniform | 1 days |

Given the DS of each individual bridge, the trajectory of the post-shock functionality recovery of the RN is tracked since the beginning of IAoEs, driven by the two agents described above. In each MC realization, their behavioural attributes are randomly sampled from probabilistic distributions characterized by predefined

parameters. As shown in Table 1, regarding Agent A, $V_{er}$, as the attribute of the travel velocity, is assumed to follow a uniform distribution with the lower and upper limits of 15km/h and 20km/h, respectively. This relatively low speed accounts for the potential impact of the debris and traffic jams in the IAoEs. In parallel, regarding Agent B, who runs the FR and might need to transport heavy equipment, its travel velocity, *i.e.*, $V_{fr}$, ranges between 5 km/h and 10 km/h. In terms of the restoration efficiency, $E_{er}$ of Agent A follows a uniform distribution with the lower and upper limit of 50%/day and 100%/day, respectively. Therefore, the expected time to complete the ER of an individual collapsed bridge will range from 1 to 2 days. Nonetheless, it is important to note that this parameter is reduced following Eq. (5), pursuant to the system-level damage status of the RN, at each decision-moment. In this paper, the value of ω is set to 0.45 for damaged bridges (in either DS2 or DS3) and 0.9 for partially restored bridges. Similarly, the efficiency parameter of Agent B, denoted as $E_{fr}$, also obeys a uniform distribution, with the corresponding lower and upper bounds presented in Table 1.

It is noteworthy that, regarding moderately-damaged bridges with PSI, $E_{fr}$ is replaced by $IE_{fr}$ to account for the improved recoverability, as mentioned in the Section 2.3.2. As shown in Table 1, the lower and upper bounds of $IE_{fr}$ increase substantially—from 5%–10% per day to 66.67%–200% per day—resulting in an expected restoration time of 1 day.

Finally, given the $OPL_{expected}$ and $OPL_{extreme}$ derived following Eq. (9) and Eq. (11), respectively, the resilience of the RN is quantitatively assessed. The WCL metric serves as the performance indicator, benchmarking the proposed **SBDM** framework against the two "greedy" PSI strategies, under the test scenarios involving Epicentres Nos. 1, 2, and 6. In addition, the resilience of the RN under a no-PSI scenario is also included as a baseline, thereby underscoring the improvements achieved through the PSI.

## 4. Simulation outcomes

In this Section, initially, both $OPL_{expected}$ and $OPL_{extreme}$ outlined in Section 2.5 are presented and compared against those derived from the two "greedy" strategies. Subsequently, seismic resilience of the RN is assessed under each of the four PSI lists, as well as a no-PSI scenario. Besides, all assessments are conducted in accordance with Modules 2 and 3 described in Section 2, thereby ensuring a "level playing field" across all cases.

### 4.1. The PSI lists generated

In this section, the PSI lists generated by the **SBDM** framework and the two greedy strategies are presented in both Table 2 and Fig. 4. As illustrated in Figs. 4(a) and 4(b), the bridges selected by the criticality-driven strategy are all located along the main arterial route of the RN, underscoring their pivotal role in preserving

overall network connectivity. In contrast, the fragility-driven strategy yields a more geographically dispersed selection, with bridges primarily situated in peripheral areas—demonstrating a focus on structural vulnerability rather than network connectivity.

Table 2. The recommend PSI lists.

| $OPL_{expected}$ | $OPL_{extreme}$ | Criticality-driven | Fragility-driven |
|---|---|---|---|
| 99 | 99 | 56 | 9 |
| 1 | 1 | 69 | 12 |
| 4 | 4 | 61 | 4 |
| 88 | 88 | 62 | 116 |
| 116 | 56 | 70 | 117 |

With respect to the **SBDM** framework, the optimal PSI lists under expected and extreme conditions—$OPL_{expected}$ and $OPL_{extreme}$, respectively—share four common bridges. These are spatially distributed across the northeastern, southwestern, and southern regions, indicating a deliberately dispersed intervention strategy. The sole point of divergence between the two lists is Bridge No. 56, which is included in $OPL_{extreme}$ but excluded from $OPL_{expected}$. As shown in Fig. 4(d), Bridge No. 56 is located on the main artery near the geographic centre of the RN and exhibits the highest betweenness centrality among all the 118 bridges. Its failure would thus not only result in a significant increase in the overall connectivity loss but also introduce a bottleneck effect that could hinder the system-wide recovery. Meanwhile, fragility analysis indicates that this bridge is structurally robust. In contrast, as illustrated in Fig. 4(c), $OPL_{expected}$ opts for Bridge No. 116—a seismically vulnerable structure located in the southwestern region—highlighting a prioritization shift under expected-case conditions.

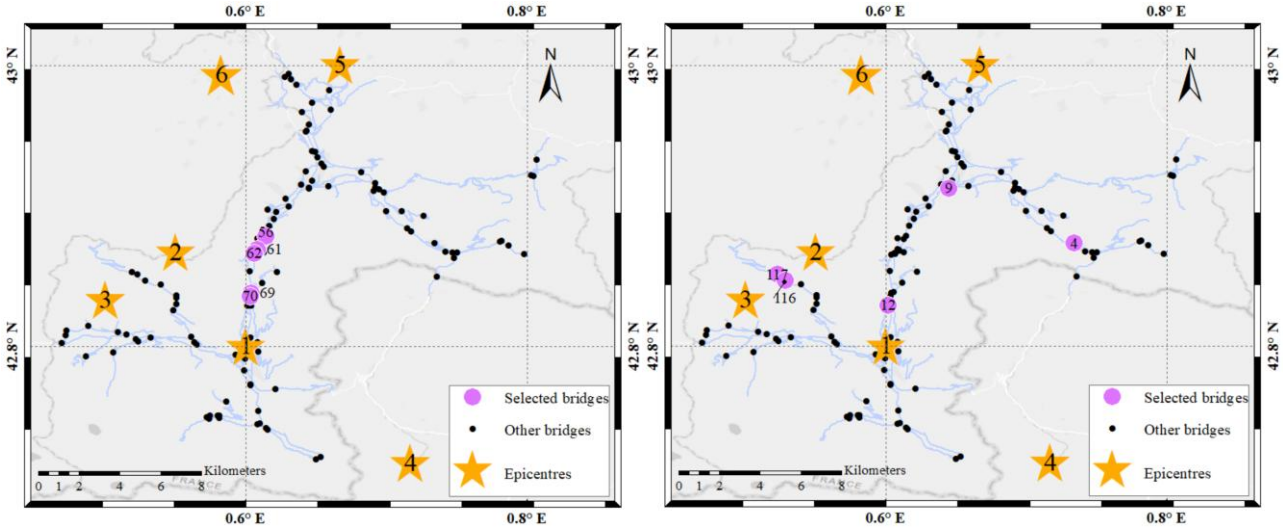


(a) Criticality-driven

(b) Fragility-driven

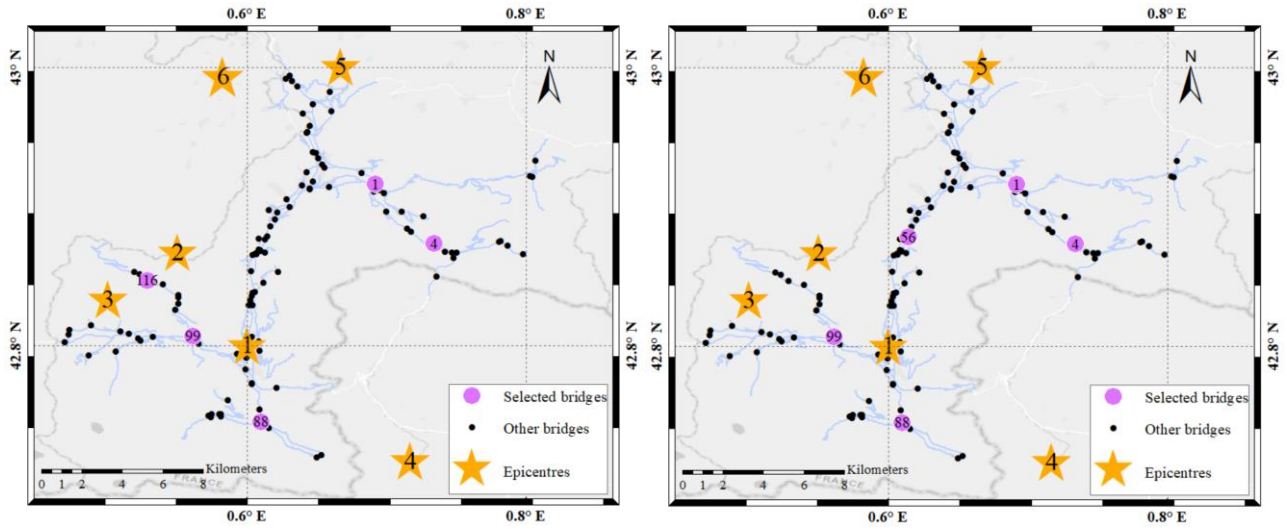


(c) $OPL_{expected}$ (d) $OPL_{extreme}$

Figure 4. The recommend PSI lists of four strategies.

Notably, among the five most "promising" bridges across the entire network (*i.e.*, Nos. 99, 1, 56, 88, and 111), measured by their WPI values—three and four ones have been picked by $OPL_{expected}$ and $OPL_{extreme}$, respectively. By comparison, the criticality-driven strategy includes only one of these top-ranked bridges, *i.e.*, Bridge No. 56, while the fragility-driven strategy includes none.

These findings underscore the stark contrast in prioritization outcomes across the different strategies. While the greedy approaches focus narrowly on either structural fragility or network criticality, the **SBDM** framework adopts a more holistic perspective—suggesting a more balanced and potentially more insightful basis for decision-making.

## 4.2. Resilience with respect to the different PSI lists

The findings presented in Section 4.1 are further substantiated by the resilience behaviour of the RN under the earthquake scenarios included in the test set, *i.e.*, the Epicentre Nos. 1, 2, and 6, as illustrated in Fig. 3. To avoid trivial simulation outcomes, the magnitude of the earthquake associated with each of the three epicentres is uniformly set to 7.0, *i.e.*, the maximum one, in this Section. Among these scenarios, Epicentre No. 1 is expected to induce the most widespread and severe damage. Accordingly, for conciseness, the time-varying analysis focuses on this scenario alone, tracking the median number of bridges in both DS2 and DS3. Figure 5 presents the corresponding result of the baseline case, *i.e.*, no-PSI, which are then compared against the resilience behaviour of the RN under each of the four distinct PSI lists.

Across all PSI strategies, a consistent reduction in earthquake-induced damage and an acceleration in the post-shock recovery of the RN are observed relative to the no-PSI baseline.

Quantitatively, under the no-PSI condition, 19 bridges fall into DS3 and 12 into DS2. In contrast, the number of DS3 bridges is reduced to 17 under the $OPL_{expected}$, $OPL_{extreme}$, and the list derived from the fragility-driven strategy. The criticality-driven strategy, however, results in 18 DS3 bridges—a less significant improvement over the baseline. Notably, none of the PSI strategies reduce the number of DS2 bridges, except for the fragility-driven one, which increases this count by one. This suggests that the DS of some of the most seismically-vulnerable bridges have been transformed from DS3 to DS2, owing to the targeted PSI following the fragility-driven strategy.

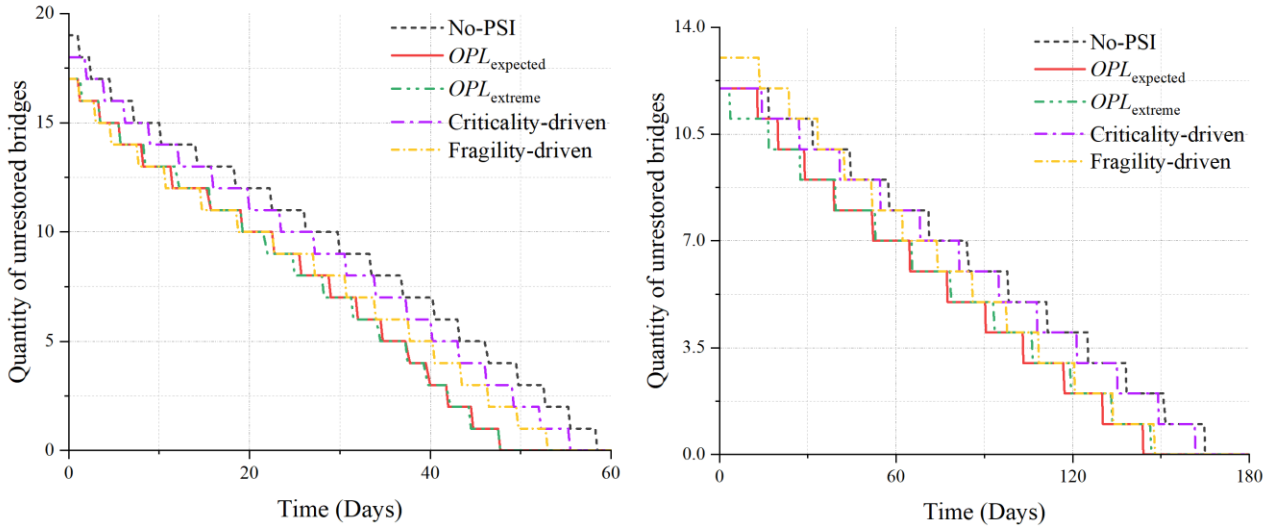


(a) DS3 (b) DS2

Figure 5. Time-varying median quantity of bridges in different DSs under the scenario with Epicentre No. 1.

Although the initial numbers of bridges in DS3 and DS2 are relatively similar across all strategies, the temporal evolution of the emergency response (ER) and full recovery (FR) campaigns diverges substantially. For instance, while the fragility-driven and search-based strategies exhibit overlapping ER trajectories at the early stage, the former increasingly lags behind midway through the campaign. As shown in Table 2 and Fig. 4, the three bridges uniquely prioritized by the fragility-driven strategy (Nos. 9, 12, and 117) exhibit low betweenness centrality, indicating limited cruciality to the overall network connectivity. This undermines the efficiency of both ER and FR efforts. Consequently, as depicted in Fig. 5(b), the FR progress under the fragility-driven strategy significantly trails that of $OPL_{expected}$ and $OPL_{extreme}$ for most of the campaign, thereby compounding delays in the associated ER.

Conversely, the $OPL_{expected}$ and $OPL_{extreme}$ prioritize bridges such as Nos. 99 and 88, which could otherwise collapse and severely impede the recovery of other damaged bridges. This targeted PSI therefore facilitates a better coordination between ER and FR campaigns, as shown in Fig. 5(a).

Lastly, the criticality-driven strategy, by neglecting the most fragile bridges, results in a higher initial number of DS3 bridges and the slowest ER progression among all the strategies. This oversight also restricts the access to numerous DS2 bridges during the FR campaign due to the presence of collapsed structures, as illustrated in Fig. 5(b). The resulting bottlenecks further diminish the effectiveness of PSI following this strategy. Furthermore, as the FR campaign progresses, the bottleneck effect imposed by collapsed bridges exacerbates these challenges, allowing the fragility-driven strategy—which begins with a higher number of DS2 bridges—to surpass the criticality-driven strategy, in the end.

Moreover, although the fragility-driven strategy initially lags behind $OPL_{expected}$ and $OPL_{extreme}$ in FR progress, it gradually narrows the gap. This is attributable to the betweenness-based heuristic followed by both Agents A and B across all five scenarios, which schedules low-betweenness bridges for later recovery. While this results in a slower initial FR, the benefits of PSI gradually materialize, as discussed in Section 2.3.2. Consequently, the fragility-driven strategy is able to partially catch up with the search-based one, consistent with the trends observed in Fig. 5(b).

Ultimately, the search-based strategy enables the most rapid execution of both ER and FR campaigns. Specifically, under both $OPL_{expected}$ and $OPL_{extreme}$, the ER duration is reduced from 58.5 days (no-PSI) to 47.75 days—a reduction of 18.4%. Similarly, the FR is completed by the 144$^{th}$ and 146.75$^{th}$ day, respectively, suggesting reductions of 12.7% and 11.1% compared to the 165-day duration under the no-PSI scenario.

Table 3. WCLs under the earthquake scenario with Epicentre No.1 ($10^3$).

| | **No-PSI** | | **PSI lists** | | | | | | | |
|---|---|---|---|---|---|---|---|---|---|---|
| | | | ***OPL*$_{expected}$** | | ***OPL*$_{extreme}$** | | **Criticality-driven** | | **Fragility-driven** | |
| | **MCs** | **Fitted** | **MCs** | **Fitted** | **MCs** | **Fitted** | **MCs** | **Fitted** | **MCs** | **Fitted** |
| **Median** | 0.819 | 0.814 | 0.572 | 0.570 | 0.556 | 0.559 | 0.708 | 0.711 | 0.708 | 0.721 |
| **75$^{th}$** | 1.044 | 1.057 | 0.776 | 0.779 | 0.745 | 0.740 | 0.884 | 0.890 | 0.927 | 0.946 |
| **95$^{th}$** | 1.547 | 1.541 | 1.263 | 1.222 | 1.103 | 1.108 | 1.209 | 1.231 | 1.392 | 1.397 |

The observation above is consistent with that on the resulting WCLs, as the resilience measure. In Fig. 6, the probability density functions (PDF) following lognormal distribution, fitted to the WCL dataset from the total of 200 MC runs, have been plotted regarding the case of No-PSI and the four distinct PSI lists. In particular, a total of three quantiles, *i.e.*, the median, 75$^{th}$, and 95$^{th}$ ones, respectively, associated with the fitting and the MC simulation have also been presented and compared in Table 3. Overall, across all the cases, the discrepancy rate of the three quantiles never exceeds 5%, indicating a sufficiently accurate fitting.

As illustrated in Table 3 and Fig.6, across all the different strategies, PSI is found to have substantially enhanced seismic resilience of the RN, compared to the no-PSI baseline.

From the median standpoint, the search-based strategy has outperformed the PSI list derived from the two greedy strategies, by enabling a much more significant reduction of WCL. Specifically, the $OPL_{expected}$ and $OPL_{extreme}$ have decreased the median to 572 and 556, indicating a 30.16% and 32.11% reduction, compared to 819, as the case of no-PSI. By contrast, both two greedy strategies have decreased the value to 708, corresponding to a more modest 13.55% reduction.

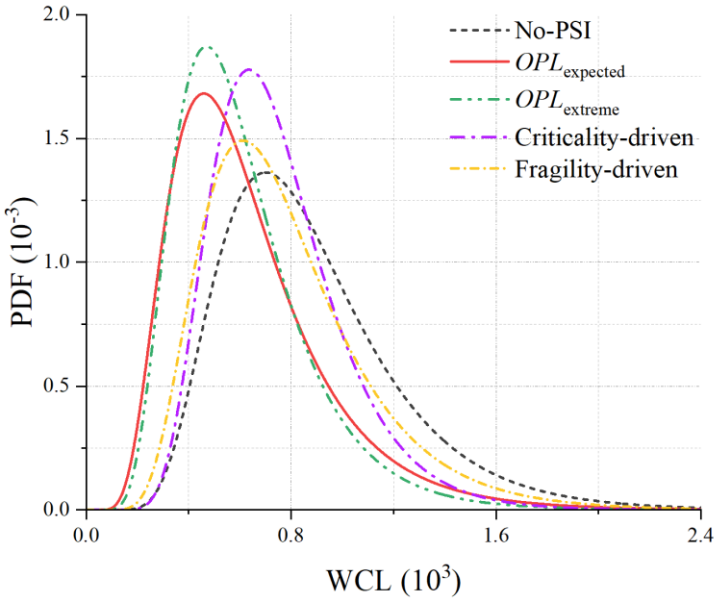


Figure 6. Probability density functions of WCL under the scenario with Epicentre No. 1.

This performance gap persists at the 75th quantile, which indicates more severe disruption scenarios. Quantitively, the $OPL_{expected}$ and $OPL_{extreme}$ have enabled reductions of 25.67% and 28.64%, lowering the WCL from 1044 (No-PSI) to 776 and 745, respectively. Meanwhile, the two greedy strategies diverge in the performance: The criticality-driven strategy achieves a 15.33% reduction, outperforming the fragility-driven one, which yields only an 11.21% reduction.

It is noteworthy that, the gap between the criticality-driven and search-based strategy narrows sharply, when it comes the increasingly extreme cases, as illustrated in Fig. 6. In particular, despite the small margin, the criticality-driven PSI even manages to outcompete the $OPL_{expected}$, leading to a WCL of 1209 that is 4.28% lower than 1263, as the case of the latter, measured at the 95th quantile.

Such a shift suggests that, prioritizing topologically critical yet seismically robust bridges (*e.g.*, Bridge No. 56), as done in the criticality-driven strategy, may contribute marginally under typical seismic scenarios. However, under extreme scenarios—such as those originating from Epicentre No. 1, which is geographically proximate to many of these bridges—the likelihood of collapse increases significantly. As discussed in Section 4.1, the failure of these bridges can result in not only substantial initial losses but also prolonged bottlenecks

that hinder the overall restoration of the RN, thereby inflating WCLs. Consequently, the criticality-driven strategy proves particularly effective in such scenarios, despite its narrower focus.

Conversely, the fragility-driven strategy yields the least improvement at the 95$^{th}$ quantile. As shown in Table 3, it results in a WCL of 1392—15.14% higher than that of the criticality-driven strategy.

Finally, the $OPL_{extreme}$, which is explicitly designed to optimize PSI under extreme conditions (as defined in Eqs. 11–12), has achieved the lowest WCL at the 95$^{th}$ quantile. By including Bridge No. 56—unlike $OPL_{expected}$—$OPL_{extreme}$ reduces WCL to 1103, indicating an 8.77% improvement over the criticality-driven strategy. Relative to the No-PSI case, this corresponds to a 28.7% reduction, underscoring the effectiveness of targeted PSI under high-impact seismic scenarios.

Table 4. WCLs under the earthquake scenario with Epicentre No.2 ($10^3$).

| | **No-PSI** | | **PSI lists** | | | | | | | |
|---|---|---|---|---|---|---|---|---|---|---|
| | | | ***OPL*$_{expected}$** | | ***OPL*$_{extreme}$** | | **Criticality-driven** | | **Fragility-driven** | |
| | **MCs** | **Fitted** | **MCs** | **Fitted** | **MCs** | **Fitted** | **MCs** | **Fitted** | **MCs** | **Fitted** |
| **Median** | 0.621 | 0.638 | 0.408 | 0.413 | 0.378 | 0.374 | 0.503 | 0.500 | 0.554 | 0.566 |
| **75$^{th}$** | 0.823 | 0.844 | 0.561 | 0.580 | 0.508 | 0.509 | 0.629 | 0.634 | 0.756 | 0.771 |
| **95$^{th}$** | 1.324 | 1.264 | 0.957 | 0.945 | 0.772 | 0.792 | 0.900 | 0.893 | 1.208 | 1.200 |

The behavioural pattern of the RN under the scenario with Epicentre No. 1 is consistent with that associated with Epicentre No. 2, where the expected damage is comparatively less severe, as presented in Table 4 and Fig. 7(a). Similarly, measured by the median, both $OPL_{expected}$ and $OPL_{extreme}$ have been leading by a significant margin. Quantitatively, the WCL has been reduced to 408 and 378, corresponding to reductions of 34.30% and 39.13%, respectively, relative to case of no-PSI (*i.e.*, 621). By comparison, the criticality- and fragility-driven strategies result in relatively moderate reductions, with the WCL values of 503 and 554, indicating improvements of 19.00% and 10.79%, respectively. The competitive edge of the search-based strategy has been maintained, at the 75$^{th}$ quantile, as shown in both Table 4 and Fig. 7(a). Meanwhile, similar to the observation under Epicentre No. 1, the criticality-driven strategy gains effectiveness under increasingly extreme conditions. At the 95$^{th}$ quantile, it leads to a WCL of 900—5.96% lower than the 957 associated with $OPL_{expected}$—indicating a reversal in the competitiveness under high-impact scenarios. Nevertheless, the criticality-driven strategy remains outperformed by $OPL_{extreme}$, which yields the lowest WCL at this quantile (772), reaffirming its advantage in extreme-event preparedness.

Fig. 7(b) presents the PDF of WCL under the earthquake scenario with Epicentre No. 6, located in the northern periphery of the network and geographically distant from its central core. As a result, the damage induced by earthquakes with this Epicentre is projected to be substantially less widespread and severe compared

to Epicentres Nos. 1 and 2. As shown in Tables 3 and 5, even at the 95$^{th}$ quantile, the WCL under Epicentre No. 6 (590) remains well below the median WCL under Epicentre No. 1(819), indicating a relatively benign seismic impact.

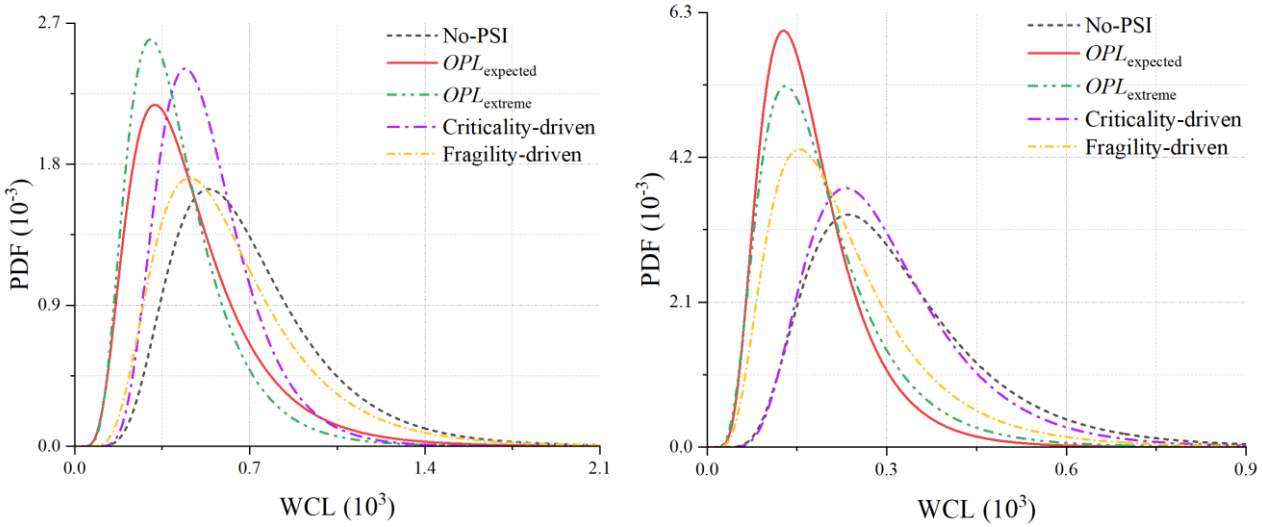


(a) Epicentre No.2 (b) Epicentre No.6

Figure 7. Probability density function of WCLs under the scenarios with Epicentres Nos.2 and 6.

Correspondingly, the resilience behaviour of the RN under this scenario diverges significantly from that observed under Epicentres Nos. 1 and 2. As demonstrated in Fig. 7(b) and Table 5, $OPL_{expected}$ consistently outperforms all the other strategies, including $OPL_{extreme}$, across all quantiles. Specifically, it reduces the WCL to 158, 220, and 328 at the median, 75$^{th}$, and 95$^{th}$ quantiles, respectively—indicating reductions of 45.52%, 42.71%, and 44.41%, compared to the No-PSI baseline values of 290, 384, and 590. Notably, under this low-impact scenario, both greedy strategies lag significantly behind the search-based ones, even at the 95$^{th}$ quantile, as shown in Fig. 7(b).

Moreover, a reversal of the competitiveness of the two strategies themselves has also been observed. Contrary to their behaviours under more severe scenarios, the fragility-driven strategy outperforms the criticality-driven one across all quantiles. Specifically, the criticality-driven strategy results in WCLs of 282, 354, and 535—exceeding those of the fragility-driven strategy (205, 277, and 473) by 37.56%, 27.80%, and 13.11%, respectively. Notably, as illustrated in Table 5 and Fig. 7(b), the criticality-driven strategy barely surpasses the No-PSI baseline when examined by the median, yielding only a marginal improvement of 2.76% (*i.e.*, 282 versus 290).

These findings therefore underscore a key insight: Overemphasizing extreme-case preparedness—as in $OPL_{extreme}$—by prioritizing structurally robust but topologically critical bridges may lead to suboptimal PSI under benign seismic scenarios, such as that associated with Epicentre No. 6. In contrast, optimizing for the

expected disruption, as in $OPL_{expected}$, better aligns with the prevailing damage patterns and yields more cost-effective resilience enhancement.

Table 5. WCLs under the earthquake scenario with Epicentre No.6 ($10^3$).

| | No-PSI | | PSI lists | | | | | | | |
|---|---|---|---|---|---|---|---|---|---|---|
| | | | $OPL_{expected}$ | | $OPL_{extreme}$ | | Criticality-driven | | Fragility-driven | |
| | **MCs** | **Fitted** | **MCs** | **Fitted** | **MCs** | **Fitted** | **MCs** | **Fitted** | **MCs** | **Fitted** |
| **Median** | 0.290 | 0.290 | 0.158 | 0.158 | 0.178 | 0.170 | 0.282 | 0.276 | 0.205 | 0.203 |
| **75$^{th}$** | 0.384 | 0.393 | 0.220 | 0.217 | 0.247 | 0.240 | 0.354 | 0.367 | 0.277 | 0.288 |
| **95$^{th}$** | 0.590 | 0.610 | 0.328 | 0.340 | 0.382 | 0.394 | 0.535 | 0.551 | 0.473 | 0.479 |

In summary, the result presented in this Sub-section highlights the inherent complexity of PSI decision-making. The case-study demonstrates that the proposed framework—by effectively balancing the fragility and criticality of components—serves as a robust tool for resilience enhancement. Particularly, by incorporating dual optimization objectives targeting both expected and extreme-case resilience behaviour, the **SBDM** framework ensures that PSI are dynamically aligned with the hazard intensity, exposure, and recoverability of CISs, thereby offering scenario-sensitive and adaptive guidance.

## 5. Conclusions

This study presents a resilience-oriented, search-based decision-making (**SBDM**) framework of selecting and scheduling pre-shock interventions (PSIs), with a specific focus on road networks (RNs) exposed to seismic hazards. In this context, seismic performance enhancement of bridge structures—deemed the weakest link in modern RNs—has been adopted as a viable PSI approach. Accordingly, a subset of bridges in a RN is selected and scheduled for fragility and recoverability enhancement. These interventions aim to reduce the seismic vulnerability of bridges while accelerating the restoration of the RN in the IAoEs.

To capture the dynamic impact of PSI on the RN's recovery, a dedicated agent-based model (ABM) is developed and integrated into the **SBDM** framework. In this ABM, each recovery team involved in the emergency restoration campaign is modelled as an agent, whose behaviour is governed by predefined attributes. Accordingly, the **SBDM** framework enables a nuanced assessment on how each PSI list reshapes both vulnerability and recoverability of the RN. Ultimately, by incorporating two distinct optimization objectives—minimizing the expected and the 95$^{th}$ quantile of the weighted connectivity loss (a resilience measure of the RN) the proposed framework systematically explores the entire PSI search space and identifies the optimal list tailored to each objective.

To validate its applicability, the **SBDM** framework is employed to guide the PSI to a real-world RN, serving as a testbed. Two different optimization objectives are fulfilled by the framework to derive two distinct optimal PSI lists. Furthermore, these lists are benchmarked against those obtained through two "greedy" strategies, the fragility- and criticality-driven ones, respectively. The resilience behaviour of the RN under all four PSI strategies is then assessed and compared to a no-PSI baseline, under an array of diverse earthquake scenarios. Based on the case-study result, the main conclusions can be drawn, as the follows:

- Across all strategies, the implementation of PSI consistently enhances seismic resilience of the RN compared to the no-PSI baseline;
- The proposed search-based PSI selection strategy outperforms both greedy strategies across a broad spectrum of seismic scenarios, demonstrating a superior adaptability;
- The proposed **SBDM** framework effectively balances the trade-off between structural vulnerability and network criticality, whereas the greedy strategies focus exclusively on one of these dimensions;
- Tailoring PSI decision-making to specific optimization objectives is essential to align with the diverse priorities of stakeholders.

Overall, the findings underscore the adaptability and robustness of the proposed framework, establishing it as a viable decision-support tool for PSI planning of RNs under uncertain and evolving seismic risks. To further advance its real-world applicability, it is strategically important to incorporate stakeholder insights into the decision-making, which will help to develop actionable and participatory resilience enhancement strategies. In parallel, future extensions should also integrate road segment damage into the PSI planning loop to adapt the framework to multi-hazard contexts.

Finally, modern critical infrastructure systems (CISs) operate as highly interconnected and interdependent networks, where the failure of one component can trigger cascading disruptions and complicate recovery efforts (Zhao and Sun, 2021). These complexities highlight the need for a holistic and adaptive PSI decision-making approach—one that accounts for interdependencies and anticipates cascading failures to ameliorate CIS resilience under natural hazards. By advancing such a forward-looking framework, this research lays the groundwork for more integrated, robust, and anticipatory risk mitigation strategies tailored to the growing complexity of tomorrow's CISs.

## References

Aktas, Y. D., So, E., Johnson, C., and Cabuk, E. et al. (2023). Hybrid EEFIT Mission to February 2023 Kahramanmaraş Earthquake Sequence. *Proceedings of the SECED 2023 Conference Earthquake Engineering & Dynamics for a Sustainable Future, Society for Earthquake and Civil Engineering Dynamics (SECED), Cambridge, United Kingdom*.

Arslanturkoglu, S., and Stojadinovic, B. (2022). Seismic fatality risk evaluation framework for existing buildings in Switzerland. *Bulletin of Earthquake Engineering* 21(2): 1229-1271.

Bashan, A., Berezin, Y., Buldyrev, S. V., and Havlin, S. (2013). The extreme vulnerability of interdependent spatially embedded networks. *Nature Physics* 9(10): 667-672.

Bhattacharjee, G., and Baker, J. W. (2023). Using global variance-based sensitivity analysis to prioritise bridge retrofits in a regional road network subject to seismic hazard. *Structure and Infrastructure Engineering* 19(2): 164-177.

Brandes, U. (2001). A faster algorithm for betweenness centrality. *Journal of Mathematical Sociology* 25(2): 163-177.

Brummitt, C. D., D'Souza, R. M., and Leicht, E. A. (2012). Suppressing cascades of load in interdependent networks. *Proceedings of the National Academy of Sciences* 109(12): E680-E689.

Buldyrev, S. V., Parshani, R., Paul, G., Stanley, H. E., and Havlin, S. (2010). Catastrophic Cascade of Failures in Interdependent Networks. *Nature* 464(7291): 1025-1028.

Bruneau, M., Chang, S. E., and Eguchi, R. T. et al. (2003). A framework to quantitatively assess and enhance the seismic resilience of communities. *Earthquake Spectra* 19(4): 733-752.

Campbell, K. W., and Bozorgnia, Y. (2008). NGA ground motion model for the geometric mean horizontal component of PGA, PGV, PGD and 5% damped linear elastic response spectra for periods ranging from 0.01 to 10 s. *Earthquake Spectra* 24 (1): 139-171.

Carturan, F., Pellegrino, C., Rossi, R., Gastaldi, M., and Modena, C. (2013). An integrated procedure for management of bridge networks in seismic areas. *Bulletin of Earthquake Engineering* 11(2): 543-559.

Chang, L., Peng, F., Ouyang, Y., Elnashai, A. S., and Spencer, B. F. (2012). Bridge seismic retrofit program planning to maximize postearthquake transportation network capacity. *Journal of Infrastructure Systems 18*(2): 75-88.

Costa, R., Haukaas, T., and Chang, S. E. (2021). Agent-based model for post-earthquake housing recovery. *Earthquake Spectra* 37(1): 46-72.

Dong, Y., Frangopol, D. M., and Saydam, D. (2014). Pre-earthquake multi-objective probabilistic retrofit optimization of bridge networks based on sustainability. *Journal of Bridge Engineering* 19(6): 04014018.

Druckenmiller, H., Liao, Y. J., Pesek, S., Walls, M., and Zhang, S. (2024). Removing development incentives in risky areas promotes climate adaptation. *Nature Climate Change* 14: 936-942.

El-Hawat, O., Fatahi, B., and Taciroglu, E. (2022). Novel post-tensioned rocking piles for enhancing the seismic resilience of bridges. *Earthquake Engineering & Structural Dynamics* 51(2): 393-417.

Galasso, C., and Opabola, E. A. (2024). The 2023 Kahramanmaraş Earthquake Sequence: finding a path to a more resilient, sustainable, and equitable society. *Communications Engineering* 3(1): 24.

Gehl, P., and D'Ayala, D. (2018). System loss assessment of bridge networks accounting for multi-hazard interactions. *Structure and Infrastructure Engineering* 14(10): 1355-1371.

Huang, Y., Parmelee, S., and Pang, W. (2014). Optimal retrofit scheme for highway network under seismic hazards. *International Journal of Transportation Science and Technology 3*(2): 109-128.

Helbing, D. (2013). Globally networked risks and how to respond. *Nature* 497(7447): 51-59.

Jafari, L., Khanmohammadi, M., Capacci, L., & Biondini, F. (2024). Resilience-Based Optimal Seismic Retrofit and Recovery Strategies of Bridge Networks under Mainshock–Aftershock Sequences. *Journal of Infrastructure Systems 30*(3): 04024015.

Karim, K. R., and Yamazaki, F. (2003). A simplified method of constructing fragility curves for highway bridges. *Earthquake Engineering & Structural Dynamics* 32(10): 1603-1626.

Kilanitis, I., and Sextos, A. (2019). Impact of earthquake-induced bridge damage and time evolving traffic demand on the road network resilience. *Journal of Traffic and Transportation Engineering (English Edition)* 6(1): 35-48.

Lei, X. M., Sun, L. M., and Xia, Y. (2021). Seismic fragility assessment and maintenance management on regional bridges using Bayesian multi-parameter estimation. *Bulletin of Earthquake Engineering* 19(15): 6693-6717.

Luo, H., and Paal, S. G. (2021). Advancing post-earthquake structural evaluations via sequential regression-based predictive mean matching for enhanced forecasting in the context of missing data. *Advanced Engineering Informatics* 47: 101202.

Luo, Z., Zhang, W. X., Chen, Y., and Liu, Y. H. (2025). Seismic performance and repairability of the rocking piers with elliptical bottoms. Structures 75: 108649.

Mackie, K. R., and Stojadinovic, B. (2006). Post-earthquake functionality of highway overpass bridges. *Earthquake Engineering & Structural Dynamics* 35(1): 77-93.

Mackie, K. R., Wong, J. M., and Stojadinovic, B. (2010). Post-earthquake bridge repair cost and repair time estimation methodology. *Earthquake Engineering & Structural Dynamics* 39(3): 281-301.

Magoua, J. J., Wang, F., Li, N., and Fang, D. P. (2023). Incorporating the human factor in modeling the operational resilience of interdependent infrastructure systems. *Automation in Construction* 149: 104789.

Martins, L., and Silva, V. (2021). Development of a fragility and vulnerability model for global seismic risk analyses. *Bulletin of Earthquake Engineering* 19(15): 6719-6745.

Mesta, C., Ceferino, L., Cremen, G., and Galasso, C. (2025). Investigating post-earthquake hospital transportation for casualties through agent-based modeling. *Earthquake Spectra*, accepted.

Nicholson, C., Tehrani, M. H., and Ghasemkhani, A. (2024). A systemic approach for assessing infrastructure component importance in hazard-prone communities. *International journal of disaster risk reduction* 113: 104880.

Nie, L., Jiang, L., Zhou, W., Jiang, Z., Feng, Y., and Lai, Z. (2025). Quasi-static testing of rocking piers for railway bridges. *Engineering Structures* 332: 120110.

Noh, H. Y., Jaiswal, K. S., Engler, D., and Wald, D. J. (2020). An efficient Bayesian framework for updating PAGER loss estimates. *Earthquake Spectra* 36(4): 1719-1742.

Sharif, S. V., Moshfegh, P. H., and Kashani, H. (2023). Simulation modeling of operation and coordination of agencies involved in post-disaster response and recovery. *Reliability Engineering* and *System Safety* 235: 109219.

Shen, Y., Freddi, F., Li, Y., and Li, J. (2024). Shaking table tests of seismic-resilient post-tensioned reinforced concrete bridge piers with enhanced bases. *Engineering Structures* 305: 117690.

Shinozuka, M., Feng, M. Q., Kim, H. K., Uzawa, T., and Ueda, T. (2003). Statistical analysis of fragility curves. *Technical report MCEER-03-0002*. *http://shinozuka.eng.uci.edu/Pdf/RepFrag.pdf*

Silva-Lopez, R., Baker, J. W., and Poulos, A. (2022). Deep learning-based retrofitting and seismic risk assessment of road networks. *Journal of Computing in Civil Engineering* 36(2): 04021038.

Sun, L. (2017). *Modeling the seismic resilience of electric power supply systems*. Ph.D. Thesis, Department of Civil, Environmental and Geomatic Engineering, Swiss Federal Institute of Technology Zurich (ETH Zurich), Switzerland.

Sun, L., D'Ayala, D., Fayjaloun, R., and Gehl, P. (2021). Agent-based model on resilience-oriented rapid responses of road networks under seismic hazards. *Reliability Engineering and System Safety* 216: 108030.

Sun, L., Shawe-Taylor, J., and D'Ayala, D. (2022). Artificial intelligence-informed planning for the rapid response of hazard-impacted road networks. *Scientific Reports* 12(1): 16286.

Sun, L., Shawe-Taylor, J., Yang, S., and Stojadinović, B. (2025). Lookahead strategies for planning of post-disaster emergency restoration of road networks. *International Journal of Disaster Risk Reduction* 126: 105648.

Thacker, S., Adshead, D., Fay, M., Hallegatte, S., Harvey, M., Menus, H., O'Regan, N., Rozenberg, J., Watkins, G., and Hall, J. W. (2019). Infrastructure for sustainable development. *Nature Sustainability* 2(4): 324-331.

Venkittaraman, A., and Banerjee, S. (2014). Enhancing resilience of highway bridges through seismic retrofit. *Earthquake Engineering & Structural Dynamics* 43(8): 1173-1191.

Woessner, J., Danciu, L., Kaestli, P., & Monelli, D. (2013). D6.6-Database of seismogenic zones, Mmax, earthquake activity rates, ground motion attenuation relations and associated logic trees. *Seismic Hazard Harmonization in Europe (SHARE) Project Deliverable. http://www.efehr.org/export/sites/efehr/.galleries/dwl_europe2013/D6-6_SHAREopt.pdf_2063069299.pdf*

Wu, Y. Y., and Chen, S. (2023). Resilience modeling and pre-hazard mitigation planning of transportation network to support post-earthquake emergency medical response. *Reliability Engineering & System Safety* 230: 108918.

Yeh, F. Y., Chang, K. C., Sung, Y. C., Hung, H. H., and Chou, C. C. (2015). A novel composite bridge for emergency disaster relief: Concept and verification. *Composite Structures* 127: 199-210.

Zampieri, P. (2014). *Simplified seismic vulnerability assessment of masonry arch bridges*. Ph.D. Thesis, University of

Trento, Italy.

Zhang, L. L., Liu, X., Li, Y. P., Liu, Y., Liu, Z. P., Lin, J. C., Shen, J., Tang, X. F., Zhang, Y., and Liang, W. N. (2012). Emergency medical rescue efforts after a major earthquake: lessons from the 2008 Wenchuan earthquake. *The Lancet* 379(9818): 853-861.

Zhang, W., and Wang, N. (2016). Resilience-based risk mitigation for road networks. *Structural Safety* 62:57-65.

Zhao, T., and Sun, L. (2021). Seismic resilience assessment of critical infrastructure-community systems considering looped interdependences. *International Journal of Disaster Risk Reduction* 59: 102246.

Zhao, T., Wang, J., and Sun, L. (2023). Crowd dynamic-based model on the city-wide emergency transfer under catastrophic earthquakes. *International journal of disaster risk reduction* 93: 103777.